A Low-Profile Miniaturized Frequency Selective Surface with Insensitive Polarization

Meiyu Wang [1], Lei Zhao [2*], Jun Wang [2], Xinhua Liang [3], Shengjun Zhang [4], Yingsong Li [1], and Wenhua Yu [2]

[1] College of Information and Communication Engineering
Harbin Engineering University, Harbin, 150001, China

[2] Center for Computational Science and Engineering, School of Mathematics and Statistics
Jiangsu Normal University, Xuzhou, China
*leizhao@jsnu.edu.cn

[3] School of Physics Electronic Engineering, Jiangsu Normal University, Xuzhou, China

[4] National Key Laboratory of Science and Technology on Test Physics & Numerical Mathematical, Beijing, China

Abstract ─ In this letter, a low-profile miniaturized broadband bandpass frequency selective surface (FSS) is proposed. The proposed structure consists of a convoluted dipole metal layer and its complementary pattern, which are separated by a dielectric substrate with a thickness of $0.003\lambda_0$, where λ_0 is the resonant wavelength in free space. The cell size of the proposed FSS is only $0.03\lambda_0 \times 0.03\lambda_0$. Furthermore, 3 dB bandwidth of the proposed FSS is approximately 50% for the normal incidence. Low profile and miniaturization of the structure element contribute to the great stability of frequency response under the incident waves with different incident angles and polarizations. To better understand the operational principle of the proposed FSS, the equivalent circuit model is presented. The proposed FSS prototype was fabricated and measured to validate the design.

Index Terms ─ Angular stability, frequency selective surface, miniaturization, wideband

I. INTRODUCTION

Frequency selective surfaces (FSSs) as spatial filters have been extensively studied in the past decades, and they have been widely used for antennas, radomes, satellite communications, electromagnetic interference (EMI) shielding and other microwave and millimeter wave applications [1-3]. Due to the space constraints in practical applications, it is necessary to include enough number of unit cells in a finite space to achieve the similar performance as in an infinite space. In addition, reducing cell size cannot only delay the generation of grating lobes, but also reduce the distortion in conformal surfaces. Recently, a large number of studies have been focusing on miniaturization of the unit cell, and many techniques are proposed to achieve miniaturization. The miniaturization of the unit cell can be expressed as reducing the resonance frequency without changing the unit size.

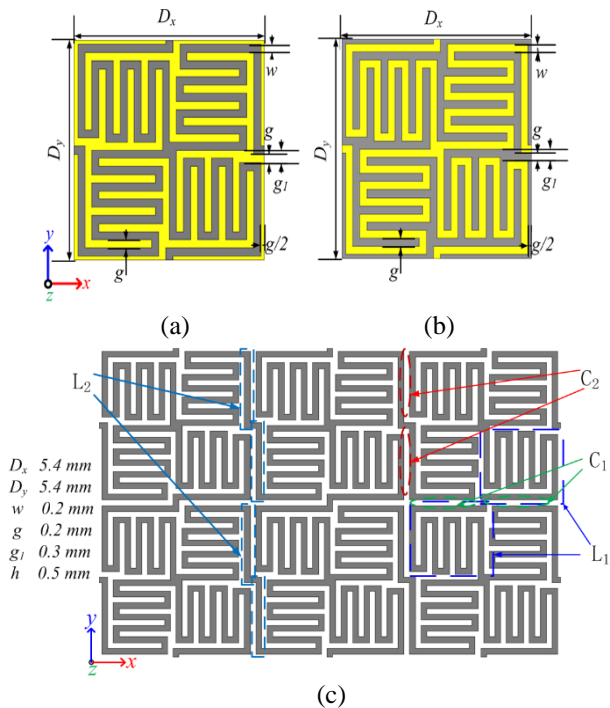|	
D_x	5.4 mm
D_y	5.4 mm
w	0.2 mm
g	0.2 mm
g_1	0.3 mm
h	0.5 mm

Fig. 1. Geometry of the proposed FSS. (a) Top layer element. (b) Bottom layer element. (c) Top layer structure and parameter description.

It is well known that the resonant frequency reduction needs to increase the inductance and capacitance values of the equivalent circuit. In [4], a class of bandpass FSSs were proposed, which were made up of metallic patches separated by a thin substrate backed by a wire mesh with the same periodicity. The unit size of the structure does not depend on a half resonant wavelength. By minimizing the line width and gap, the cell size can be greatly reduced. With the interweaving technique proposed in [5], the convoluted cross dipole is modified to interweaved with its neighbors to reduce resonant frequency. The miniaturized FSS using 2.5D closed loop connected in series by four vias is provided in [6]. The miniaturization of the 2.5D structure is achieved by expanding the 2D structure to 2.5D in space, increasing inductances in the unit cell and capacitance between the adjacent cells through vias. Another alternative method is to add lumped elements directly between the gaps in the structures [7]. Because the lumped components require soldering and their own stability requirements, this method can only be used in particular environments.

In addition, multilayer [8] and convoluted structures [9] are also provided for miniaturization. In [10], two layers on two sides of a substrate are arranged orthogonal to each other for generating a very strong cross-layer capacitance to achieve miniaturization that can miniaturize the element size much further. An ultra-thin single-layer miniaturized-element FSS based on meander line approach is shown in [11]. Being asymmetric in nature, the structure is sensitive to polarization.

In this letter, a new miniaturized low profile bandpass FSS is proposed. Since the bandpass FSS is usually modeled as a parallel LC circuit. By using the meander line to increase the strip length, the equivalent inductance is greatly increased. The larger inductance values result in smaller resonant frequencies and wider bandwidth as resonant frequency $f_0 = 1/2\pi\sqrt{LC}$ and bandwidth $W \propto \sqrt{L/C}$. Compared to the structures mentioned above, the proposed FSS has the following advantages: 1) The unit cell size is compact, which only has $0.03\lambda_0 \times 0.03\lambda_0$; 2) The symmetry and miniaturization of the cell size as well as the thin dielectric layer together lead to more stable characteristics.

II. GEOMETRY AND EQUIVALENT CIRCUITS MODEL

Figure 1 shows the geometry of the proposed FSS, which consists of a convoluted line metallic layer etched on the top of the substrate, while its complementary pattern is laid on the back of the substrate. The gray area represents the metal layer and the yellow area represents the dielectric substrate. The element of the structure exhibits 90^0 of rotational symmetry, a quarter of which is made up of a section of meander line and a metallic

strip connecting adjacent cells. The proposed FSS is etched on a 0.5mm-thick F4B substrate with a relative dielectric constant of 2.65 and a loss tangent of 0.0015. The other design parameters of the proposed structure are given in Fig. 1.
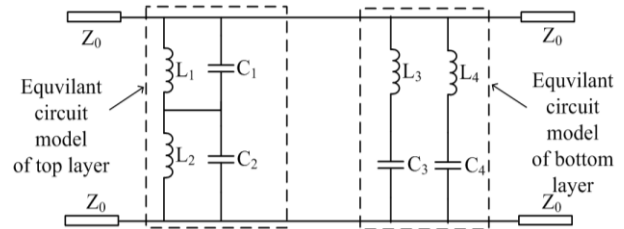

Fig. 2. Equivalent circuit model (ECM) of the proposed FSS.

The equivalent circuit model of the proposed FSS is demonstrated in Fig. 2. The effects of the top layer on total inductance and capacitance are described on the left side of Fig. 2. The equivalent circuit of the bottom layer resonator can be described as the dual form of the top layer, which is shown on the right side of Fig. 2. Under vertical polarization, the direction of the electric field is in the y-axis. The circuit of the top layer resonator without patterns on the back side describes as series of two parallel LC resonators. In the parallel resonator composed of L_1 and C_1, L_1 corresponds to the strips paralleling to the y-axis, while C_1 is generated by the cell gap perpendicular to the y-axis. L_2 and C_2 respectively represent the mutual inductance and capacitance introduced by the metallic strip between adjacent cells, which work together as a parallel resonator. The meander line increases inductance of the equivalent circuit, while the metallic strip connecting adjacent cells introducing extra inductance and capacitance, which together contribute to the miniaturized unit cell. The corresponding structural parts of the circuit parameters are shown in Fig. 1 (c).

$Z_0 = 377\Omega$ is the free space impedance. The influence of the dielectric layer has been considered for obtaining the circuit parameters of the equivalent circuit. We use the curving fitting method proposed in [13] to get the parameter values of the equivalent circuit model. The top layer resonator is used as an example to discuss the curve fitting.

Firstly, the transmission coefficient $T(\omega)$ of the FSS is obtained by using the full-wave simulation, where the impedance Z_{FSS}^s is calculated by using the following formula:

$$Z_{FSS}^s = \frac{T(\omega) \cdot Z_0}{2[1 - T(\omega)]}. \tag{1}$$

Then, the impedance of the top layer resonator can be expressed as:

$$Z^s_{FSS} = \frac{j\omega(L_1 + L_2 - \omega^2 L_1 L_2 (C_1 + C_2))}{(1 - \omega^2 L_1 C_1)(1 - \omega^2 L_2 C_2)} . \quad (2)$$

Next, we minimizes the Euclidean distance between Z^S_{FSS} and Z_{FSS} to obtain the parameters of the equivalent circuit. Finally, the ECM is achieved by using the equivalent circuit parameters. The ECM results of the designed FSS are gotten by the same method used for getting the top layer resonator, where the effects of the dielectric layer are included in the calculation results.

From the curve fitting, the parameters are gotten and listed as follows: $L_1 = 8.65$ nH, $C_1 = 0.13$ pF, $L_2 = 0.79$ nH, and $C_2 = 0.20$ pF are obtained for the top layer resonator; while $L_1 = 9.75$ nH, $C_1 = 0.12$ pF, $L_2 = 0.90$ nH, $C_2 = 0.17$ pF, $L_3 = 2.37$ nH, $C_3 = 0.62$ pF, $L_4 = 3.41$ nH, and $C_4 = 50.21$ fF are achieved for the designed FSS. From the fitting results in Fig. 3, we can observe that the equivalent circuit results for two different cases agree with the full wave simulation results.
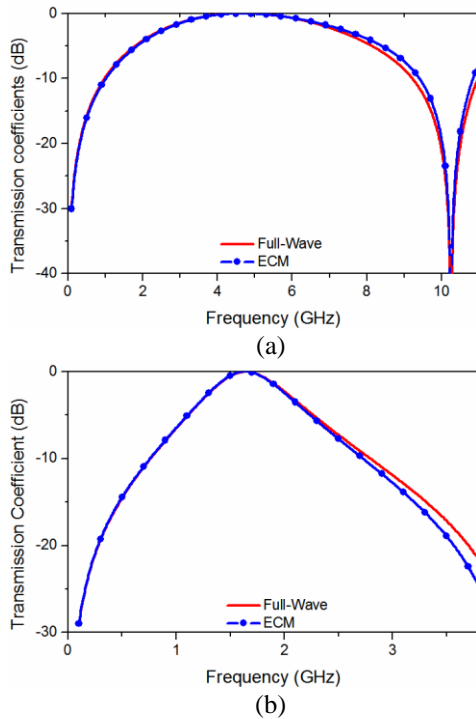

Fig. 3. Simulation and equivalent circuit results of the proposed FSS. (a) Top layer resonator without patterns on the back side. (b) Complementary FSS.

According to the description in [14], if the patch-type and slot-type FSSs (complementary structure of patch-type FSS) have the same size and are illuminated by a plane wave, the resonant frequencies of the patch elements are approximately same. If the complementary arrays are printed on both sides of a substrate, a passband with lower resonant frequency will be generated. In this letter, the proposed CFSS is used to achieve further miniaturization. Together with the ultra-wide band characters of the original slot-type resonator (top layer resonator), the proposed CFSS eventually achieved miniaturization and wideband characteristics.

III. SIMULATION AND ANALYSIS RESULTS

Full wave simulation is performed by using HFSS with the Master/Slave boundary conditions in the x- and y-directions to achieve periodicity. Floquet modes are used to excite the proposed FSS. Simulated results with different dielectric constants are shown in Table 1. The comparison of the simulation results of FSS and literature is also presented in Table 1. From Table 1, we can see that the proposed FSS has smaller unit cell and larger bandwidth than the previous results. In Table 1, FBW is 3 dB transmission bandwidth.

Table 1: Compare proposed FSS with Literature

Reference	ε_r	Unit Cell Size λ_0	f_0	FBW at Normal Incidence (%)
[8]	2.65	0.050	2.16	18.75
[9]	3	0.046	2.5	36
[4]	3.4	0.234	14	30.78
[10]	4.3	0.045	1.35	7.5
[12]	5	0.055	3.82	10.5
Proposed FSS	2.65	0.030	1.64	50.6
	3	0.028	1.57	46.5
	3.4	0.027	1.5	44.7
	4.4	0.024	1.35	40
	5	0.023	1.28	34.4

To illustrate the transmission coefficients of the proposed structure, we only take the relative dielectric constant to be 2.65 as an example. Figure 6 shows the frequency response of the proposed FSS. The detailed TE and TM transmission characteristics under oblique incidences are shown in Tables 2 and 3, respectively. From Tables 2 and 3, we can see that the maximum transmission values both appear at 1.64 GHz for TE and TM wave under the normal incidence.

Table 2: Detailed transmission characteristics of the proposed FSS for TE wave

TE					
Incident Angle (degree)	0	15	30	45	60
Resonant Frequency (GHz)	1.64	1.63	1.64	1.64	1.64
-3dB Bandwidth (MHz)	830	790	720	600	430

Table 3: Detailed transmission characteristics of the proposed FSS for TM wave

TM					
Incident Angle (degree)	0	15	30	45	60
Resonant Frequency (GHz)	1.64	1.64	1.64	1.65	1.66
-3dB Gandwidth (MHz)	830	840	950	1130	1520

Compared with the normal incidence, when the incidence angle increases to 60^0, the maximum shift of the resonant frequency is 0.6% for the TE wave, while the bandwidth is reduced from 830 MHz to 430 MHz. The maximum shift of the resonant frequency is 1.2% for the TM polarization, while its bandwidth is increased from 830 MHz to 1520MHz. It is shown that for the TE wave, the bandwidth decreases as the incident angle increases; for the TM wave, the bandwidth decreases as the incident angle increases. This is because that as the angle of incidence θ varies, for the TE wave, the impedance changes as $Z_0/\cos\theta$, and thus results in a higher loading quality factor of the resonator. For the TM wave, the impedance changes as $Z_0\cos\theta$, leading to a lower loader quality factor. Higher loading quality factor results in a narrower bandwidth, and vice versa [1, 15].

Figure 4 shows the transmission coefficients under various incident angles and polarization angles. From the figure we can see that the transmission coefficients are basically unchanged for specific incidence angle under different polarizations.

IV. EXPERIMENTAL RESULTS

In order to verify the design, the proposed FSS prototype was fabricated and measured. The fabricated FSS was printed on an F4B dielectric substrate with a relative permittivity of 2.65, which consists of 75×75 cells on both sides of the dielectric layer in an area of 405 mm $\times$ 405 mm. Figure 5 shows the photograph of the FSS measurement setup. Measurement is performed using two horn antennas (1~18 GHz) and a vector network analyzer. The FSS located between the two horn antennas that are used as the transmitting and receiving antennas. The center of the FSS is aligned with the centerline of the measurement antenna. Two measurement antennas are aligned to ensure uniform plane wave illumination on the FSS structure. In order to ensure measurement accuracy, the measurement setup is calibrated by measuring data without FSS present. Measurements with different polarizations and incidence angles are achieved by rotating the antennas and FSS structures while keeping the alignment of the central line. The measured results for oblique incident angles and different polarizations are shown in Fig. 6. It can be observed that there are some differences between the

measurement results and the simulation ones, which are mainly caused by manufacturing tolerance and measurement errors, as the measurement conditions are limited.
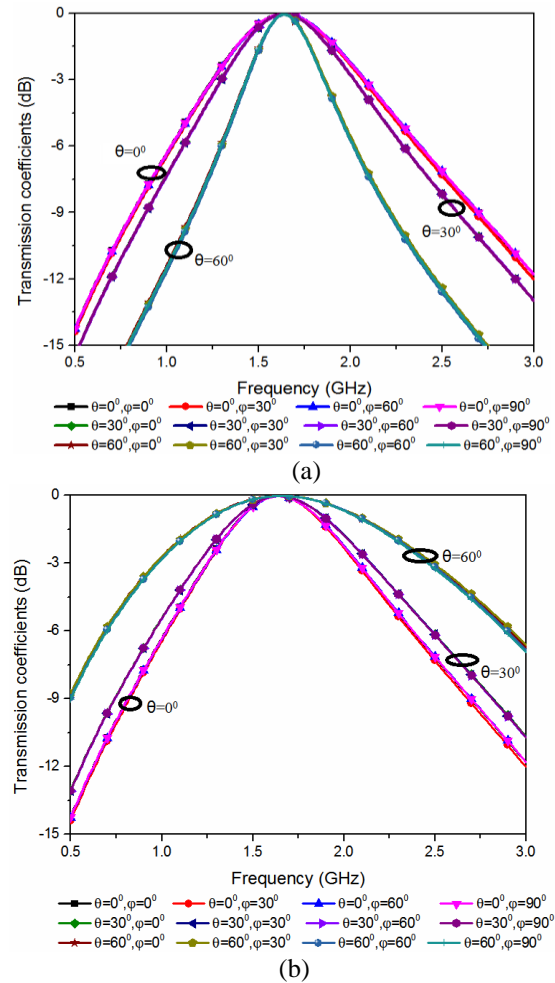

(a)

(b)

Fig. 4. Transmission coefficients under various incident angles and polarization angles. (a) TE wave incidence, and (b) TM wave incidence.
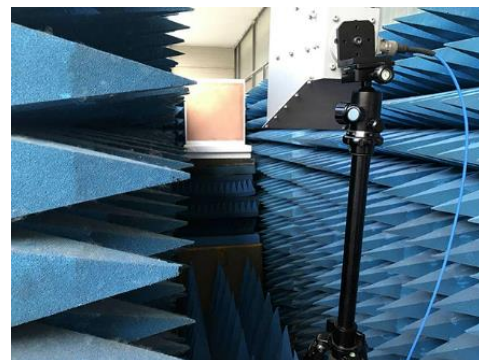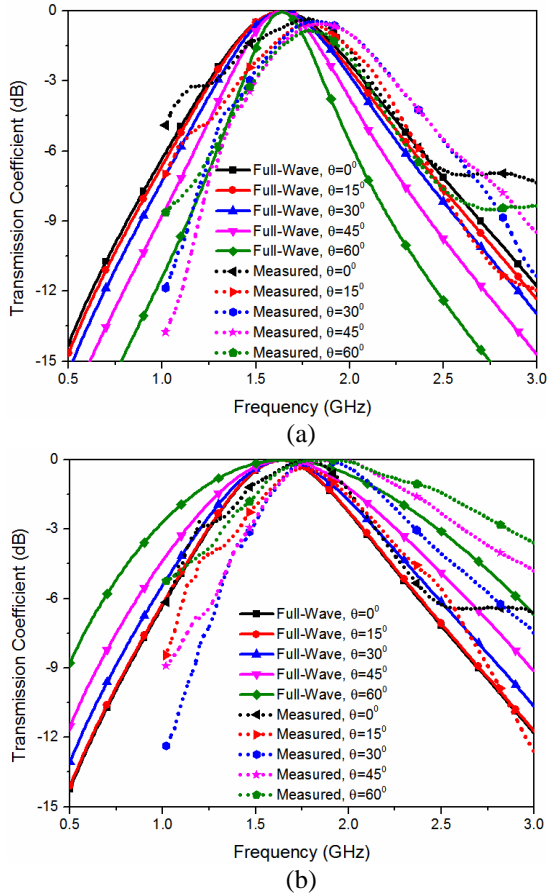

Fig. 5. Measurement setup.

Fig. 6. Simulated and measured transmission coefficients of the proposed FSS. (a) TE wave and (b) TM wave.

V. CONCLUSION

In this letter, a new low-profile FSS based on the meander line and its complementary pattern is proposed to achieve miniaturization, wide bandwidth and polarization insensitive. The unit cell size of the proposed FSS structure can be reduced to $0.03\lambda_0 \times 0.03\lambda_0$. A simple equivalent circuit model is demonstrated to illustrate the working principle of the proposed FSS.

ACKNOWLEDGMENT

REFERENCES

[1] B. A. Munk, *Frequency Selective Surfaces: Theory and Design*. New York, NY, USA: Wiley, 2000.
[2] S. Yang, J. Zhang, Y. Pang, M. Feng, and S. Qu, "Water-based metamaterial absorber for broadband electromagnetic wave absorption," *International Applied Computational Electromagnetics Society Symposium*, pp. 1-2, 2017.
[3] M. A. A. Abessolo, Y. Diallo, A. Jaoujal, A. El Moussaoui, and N. Aknin, "Stop-band filter using a new metamaterial complementary split triangle resonators (CSTRs)," *Applied Computational Electromagnetics Society Journal*, vol. 28, no. 4, pp. 353-358, 2013.
[4] K. Sarabandi and N. Behdad, "A frequency selective surface with miniaturized elements," *IEEE Trans. Antennas Propag.*, vol. 55, no. 5, pp. 1239-1245, 2007.
[5] F. Huang, J. C. Batchelor, and E. A. Parker, "Interwoven convoluted element frequency select-ive services with wide bandwidths," *Electron. Lett.*, vol. 42, no. 14, pp. 788-790, 2006.
[6] Y. R. Shi, W. Zhuang, W. C. Tang, C. Wang, and S. Liu, "Modeling and analysis of miniaturized frequency-selective surface based on 2.5-dimen-sional closed loop with additional transmission pole," *IEEE Trans. Antennas Propag.*, vol. 64, no. 1, pp. 346-351, 2016.
[7] H. L. Liu, K. L. Ford, and R. J. Langley, "Design methodology for a miniaturized frequency selective surface using lumped reactive components," *IEEE Trans. Antennas Propag.*, vol. 57, no. 9, pp. 2732-2738, 2009.
[8] H. Li, C. Yang, Q. Cao, and Y. Wang, "An ultrathin bandpass frequency selective surface with minia-turized element," *IEEE Antennas Wireless Propag. Lett.*, vol. 16, pp. 341-344, 2016.
[9] P. C. Zhao, Z. Y. Zong, W. Wu, and D. G. Fang, "A convoluted structure for miniaturized frequency selective surface and its equivalent circuit for optimization design," *IEEE Trans. Antennas Propag.*, vol. 64, no. 7, pp. 2963-2970, 2016.
[10] M. N. Hussein, J. F. Zhou, Y. Huang, M. Kod, and A. P. Sohrab, "Frequency selective surface structure miniaturization using interconnected array elements on orthogonal layers," *IEEE Trans. Antennas Propag.*, vol. 65, no. 5, pp. 2376-2385, 2017.
[11] A. B. Varuna, S. Ghosh, and K. V. Srivastava, "A miniaturized-element bandpass frequency selective surface using meander line geometry," *Microw. Opt. Techn. Lett.*, vol. 59, no. 10, pp. 2484-2489, 2017.
[12] G. Yang, T. Zhang, W. Li, and Q. Wu, "A novel stable miniaturized frequency selective surface," *IEEE Antennas Wireless Propag. Lett.*, vol. 9, pp. 1018-1021, 2010.
[13] F. Costa, A. Monorchio, and G. Manara, "Efficient analysis of frequency selective surfaces by a simple equivalent circuit approach," *IEEE Antennas Propag. Mag.*, vol. 54, no. 4, pp. 35-48, 2012.
[14] D. S. Lockyer, J. C. Vardaxoglou, and R. A. Simpkin, "Complementary frequency selective

surfaces," *IEE Proc. Microw., Antennas Propag*., vol. 147, no. 6, pp. 501-507, 2000.

[15] M. Al-Joumayly and N. Behdad, "A new technique for design of low-profile second-order bandpass frequency selective surfaces," *IEEE Trans. Antennas Propag*., vol. 57, no. 2, pp. 452-459, 2009.